

Non-collinear Spin Valve Effect in Ferromagnetic Semiconductor Trilayers

G. Xiang, M. Zhu, B. L. Sheu, P. Schiffer, and N. Samarth*

Physics Department & Materials Research Institute,
The Pennsylvania State University, University Park PA 16802

We report the observation of the spin valve effect in $(\text{Ga},\text{Mn})\text{As}/\text{p-GaAs}/(\text{Ga},\text{Mn})\text{As}$ trilayer devices. Magnetoresistance measurements carried out in the current in plane geometry reveal positive magnetoresistance peaks when the two ferromagnetic layers are magnetized orthogonal to each other. Measurements carried out for different post-growth annealing conditions and spacer layer thickness suggest that the positive magnetoresistance peaks originate in a noncollinear spin valve effect due to spin-dependent scattering at interfaces.

Heterostructures derived from ferromagnetic semiconductors (FMS) are of current interest for both fundamental and applied problems in semiconductor-based spintronics¹. In analogy to metallic spintronics, prior work has demonstrated several device configurations using the “canonical” FMS $\text{Ga}_{1-x}\text{Mn}_x\text{As}$,² including magnetic tunnel junctions,^{3,4} exchange biased bilayers⁵ and current-driven spin torque devices.⁶ However, there are no reports that show evidence of the conventional spin valve effect due to spin-dependent scattering in FMS trilayer devices. This is a phenomenon central to metal-based spintronics, and results in a giant magnetoresistance (GMR) when the magnetizations of ferromagnetic layers separated by non-magnetic *conducting* spacers switch from parallel to antiparallel states.^{7,8} The difference in resistance between these two magnetization configurations arises from corresponding differences in the contributions of spin-dependent scattering (SDS) to the electrical conductivity. A qualitative understanding of the phenomenon uses a two resistor model wherein majority and minority spins are assigned different resistivities, and where the spin diffusion length is larger than the spacer layer thickness. Based upon this picture, the magnitude of the spin valve effect is enhanced by a large difference in minority- and majority spin conductivity and by increasing the conductivity of the spacer layer.

The simple two-channel picture of the spin valve effect suggests that the phenomenon may be elusive to observation in $\text{Ga}_{1-x}\text{Mn}_x\text{As}$ -based ferromagnetic semiconductor devices because the electrical transport involves holes that have a short elastic scattering length (~ 1 nm based upon the conductivity and hole density) and – presumably – a short spin diffusion length. In addition, other sources of pronounced magnetoresistance (MR) in $\text{Ga}_{1-x}\text{Mn}_x\text{As}$ – such as the anisotropic magnetoresistance (AMR), the giant planar Hall effect (GPHE) and the anomalous Hall effect^{9,10,11} – complicate the identification of the spin valve effect. Here, we report the observation of the spin valve effect in $\text{Ga}_{1-x}\text{Mn}_x\text{As}/\text{GaAs:Be}/\text{Ga}_{1-x}\text{Mn}_x\text{As}$ trilayer devices. In strong contrast with the situation in analogous metallic devices, the associated MR in these FMS spin valves is large on an absolute scale ($\Delta R \sim 15\Omega$), but small on a relative scale ($\frac{\Delta R}{R} \sim 0.2\%$). In addition, the unusual in-plane anisotropy of $\text{Ga}_{1-x}\text{Mn}_x\text{As}$ results in spin valve

devices that show MR when the relative magnetization of the two FMS layers switches from collinear to non-collinear (orthogonal) configurations.

We fabricated $\text{Ga}_{1-x}\text{Mn}_x\text{As}/\text{GaAs:Be}/\text{Ga}_{1-x}\text{Mn}_x\text{As}$ trilayers by low temperature molecular beam epitaxy on semi-insulating (001) GaAs substrates after the growth of a 100-nm-thick standard (high temperature) GaAs buffer layer. The thickness of the $\text{Ga}_{1-x}\text{Mn}_x\text{As}$ layers is $\sim 10\text{nm}$ (calibrated using reflection high energy electron diffraction techniques) and the Mn concentration is nominally $x \sim 0.03$ (based upon earlier calibrations). The GaAs:Be spacer layer is p-doped using a Be source, with a nominal hole density $p \sim 10^{20}\text{cm}^{-3}$ and a resistivity of $\sim 10\text{m}\Omega\text{cm}$; this is based upon electrical measurements of thick Be-doped GaAs epilayers grown under identical conditions. Electrical transport measurements were carried out using dc techniques on lithographically-defined, wet-etched $500\mu\text{m} \times 200\mu\text{m}$ Hall bar mesas oriented along [110], with In contacts. We also measured the magnetization (M) of each sample using a Quantum Design superconducting quantum interference device (SQUID) magnetometer.

In order to observe spin valve behavior in such trilayers, the $\text{Ga}_{1-x}\text{Mn}_x\text{As}$ layers need to have distinct coercive fields (H_C). We accomplish this by post-growth annealing which drives hole-compensating Mn interstitials from the topmost $\text{Ga}_{1-x}\text{Mn}_x\text{As}$ layer to benign regions at the free surface of the sample;¹² in contrast, the diffusion of interstitials in the buried $\text{Ga}_{1-x}\text{Mn}_x\text{As}$ layer is believed to be self-limited by the establishment of Coulomb barriers at the GaAs/ $\text{Ga}_{1-x}\text{Mn}_x\text{As}$ interfaces. This results in clear changes to the magnetic properties of the top $\text{Ga}_{1-x}\text{Mn}_x\text{As}$ layer, while leaving the magnetic properties of the buried $\text{Ga}_{1-x}\text{Mn}_x\text{As}$ layer unaffected.^{13,14} We investigated samples with a GaAs spacer layer thickness of 2 nm, 5 nm and 10 nm: devices fabricated from these samples are identified as A, B, and C, respectively. We also studied pieces of sample B as a function of annealing time at 190° C: devices fabricated from pieces of sample B are labeled as B1, B2, B3, B4, and B5, corresponding to as-grown, and annealed for 30 min, 60 min, 90 min, 120 min, respectively. All devices fabricated from samples A and C are annealed for 60 min. Finally, as a control sample, we measured an as-grown 10 nm thick epilayer of $\text{Ga}_{1-x}\text{Mn}_x\text{As}$ with

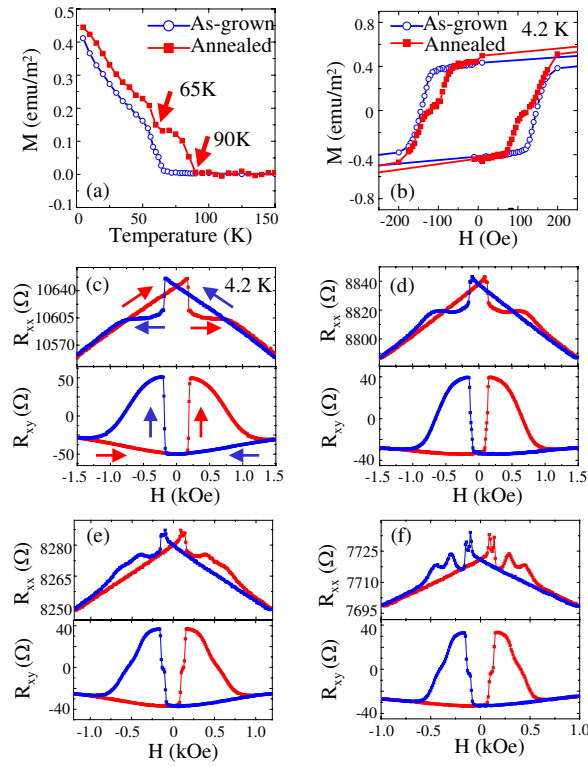


FIG. 1: Magnetization of sample B as-grown and after annealing at 190°C for 90 min as a function of (a) temperature and (b) magnetic field. Remanent magnetization in (a) was measured in a field of 30 Oe after cooling in a 10 kOe field. Magnetic field dependence of R_{xx} and R_{xy} at $T = 4.2$ K in devices fabricated from the same wafer, but subject to different annealing periods is shown in (c) Device B1: as grown; (d) device B2: annealed for 30 min; (e) device B3: annealed for 60 min; (f) device B4: annealed for 120 min. The data are all taken in the CIP geometry with $\vec{j} \parallel [110]$ and \vec{H} aligned 20° off [110].

nominally identical Mn concentration as in the trilayers (device D).

Figure 1(a) shows the temperature dependence of the remanent magnetization for devices B1 and B4 (as-grown and 90 minute anneal, respectively). The data indicate that annealing is necessary to create distinct Curie temperature (T_C) for each of the $\text{Ga}_{1-x}\text{Mn}_x\text{As}$ layers ($T_C = 65$ K for the bottom $\text{Ga}_{1-x}\text{Mn}_x\text{As}$ layer and $T_C = 90$ K for the top layer). Figure 1(b) shows that the annealing also yields a two-step $M(H)$ hysteresis loop (measured with $\vec{H} \parallel [110]$), with a distinct value of H_C for each of the $\text{Ga}_{1-x}\text{Mn}_x\text{As}$ layers. Note that the switching of the magnetization of the $\text{Ga}_{1-x}\text{Mn}_x\text{As}$ layers occurs with a 90° rotation between in-plane easy axes ($[\bar{1}00] \rightarrow [010] \rightarrow [100] \rightarrow [0\bar{1}0]$).^{9,10} Since the two $\text{Ga}_{1-x}\text{Mn}_x\text{As}$ layers do not switch simultaneously, this

results in a plateau in $M(H)$. Temperature- and field-dependent SQUID measurements of devices B1 through B5 show that the magnetic behavior of the top and bottom $\text{Ga}_{1-x}\text{Mn}_x\text{As}$ layers gradually becomes more different as a function of annealing time (data not shown).

In order to track the magnetization configurations in the trilayer, we exploit the GPHE in $\text{Ga}_{1-x}\text{Mn}_x\text{As}$ by carrying out transport measurements in the current-in-plane (CIP) geometry with the magnetic field \vec{H} deliberately misaligned with respect to the current density $\vec{j} = j\hat{x}$ at an angle ϑ . Figures 1(c) - (f) show $R_{xx}(H)$ and $R_{xy}(H)$ for devices B1, B2, B3 and B5, respectively at $T = 4.2$ K with $\vec{j} \parallel \hat{x} \parallel [110]$ and $\vartheta \sim 20^\circ$. The data for the as-grown device (B1) are similar to those for a single $\text{Ga}_{1-x}\text{Mn}_x\text{As}$ epilayer, because the two $\text{Ga}_{1-x}\text{Mn}_x\text{As}$ layers have the same T_C and H_C . However, we observe a clear qualitative change in the MR as the device is annealed: with increasing annealing time, R_{xx} shows a tendency to stand out of the MR background, eventually resulting in two pairs of double MR peaks, which must have a different origin from the AMR associated with a single $\text{Ga}_{1-x}\text{Mn}_x\text{As}$ epilayer. The annealing-induced changes to $R_{xx}(H)$ are accompanied by corresponding changes in $R_{xy}(H)$, which evolves from a one step hysteresis loop to a two-step hysteresis loop with increasing annealing time. We will argue below that the double peak MR structure is an unambiguous indication of a spin valve effect that occurs when the magnetizations of the two $\text{Ga}_{1-x}\text{Mn}_x\text{As}$ layers are orthogonal to each other. Additional evidence for the spin valve origin of these MR peaks arises from the temperature dependence of R_{xx} and R_{xy} : in Fig. 2, we show the magnetic field-dependence of R_{xx} and R_{xy} at different temperatures in device B4 with $\vec{j} \parallel \hat{x} \parallel [110]$ and $\vartheta \sim +15^\circ$. As the temperature increases, the saturated magnetization and the coercive fields of the two $\text{Ga}_{1-x}\text{Mn}_x\text{As}$ layers decrease: as a consequence, there is a decrease in the magnitudes of the jumps in both $R_{xy}(H)$ and $R_{xx}(H)$. Once the bottom layer becomes paramagnetic ($T > 60$ K), the spin valve effect vanishes, but the planar Hall effect due to the top $\text{Ga}_{1-x}\text{Mn}_x\text{As}$ layer still persists.

We now develop an analytical model of the observed behavior of $R_{xx}(H)$ and $R_{xy}(H)$ in the annealed devices. The discussion will refer to the data shown in Fig. 3 for device B4. We start with standard equations that describe the electrical field \vec{E} within a single domain ferromagnet with in-plane magnetization:¹⁰

$$E_x = j\rho_\perp + j(\rho_{||} - \rho_\perp) \cos^2 \varphi \quad (1)$$

$$E_y = j(\rho_{||} - \rho_\perp) \sin \varphi \cos \varphi \quad (2)$$

Here, φ is the angle between the current density \vec{j} along [110] and the magnetization \vec{M} ; ρ_\perp and $\rho_{||}$ are the resistivities for current flow perpendicular and parallel to the magnetization, respectively. We first determine an expression for E_y in a trilayer, noting that for an in-plane magnetic field, there is no contribution to E_y from the ordinary Hall effect and that a meaningful physical mea-

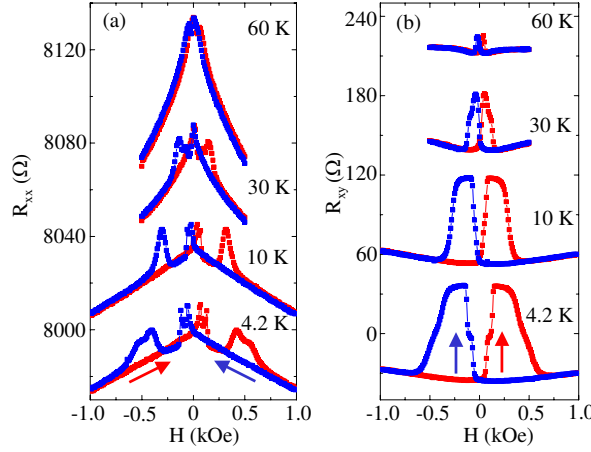


FIG. 2: Temperature dependence of (a) R_{xx} and (b) R_{xy} in device B4. The data are taken in the CIP geometry with $\vec{j} \parallel [110]$ and \vec{H} aligned 15° off [110]. The data are offset vertically for clarity.

surement of the Hall effect requires carrier accumulation on the sidewalls at equilibrium (i.e. the total transverse electrical current should be zero for the entire device). Under this condition and treating the trilayer as three parallel conductors with different resistances, the effective transverse field $(E_y)_{\text{eff}}$ is given by:

$$(E_y)_{\text{eff}} = \left[\sum_{i=1,2} \frac{j_i (\rho_{i\parallel} - \rho_{i\perp}) \sin \varphi_i \cos \varphi_i}{\rho_{i\perp} + (\rho_{i\parallel} - \rho_{i\perp}) \sin^2 \varphi_i} \right]^{-1} \times \left[\frac{1}{2\rho_0} + \sum_{i=1,2} \frac{1}{(\rho_{i\perp} + (\rho_{i\parallel} - \rho_{i\perp}) \sin^2 \varphi_i)} \right]^{-1} \quad (3)$$

Here, j_1 and j_2 are the current densities (along the x -direction by definition) in the top and bottom $\text{Ga}_{1-x}\text{Mn}_x\text{As}$ layers, respectively, and ρ_0 is the resistivity of the GaAs spacer layer. From Eq. 3, it follows that $(E_y)_{\text{eff}}$ has a minimum when the two $\text{Ga}_{1-x}\text{Mn}_x\text{As}$ layers have their magnetization parallel ($\varphi_1 = \varphi_2 = 45^\circ$). In the down-field sweep in Fig. 3(b), this corresponds to the field range between ‘‘A’’ and $H \sim -0.05$ kOe. In contrast, $(E_y)_{\text{eff}} \sim 0$ when the magnetization of the top layer is switched by the external magnetic field ($\varphi_1 = 135^\circ$ and $\varphi_2 = 45^\circ$), corresponding to ‘‘B’’ in the down sweep in Fig. 3(b). Finally, $(E_y)_{\text{eff}}$ reaches a maximum when the bottom layers magnetization switches ($\varphi_1 = \varphi_2 = 135^\circ$), corresponding to ‘‘C’’ in the down sweep in Fig. 3(b). At ‘‘D,’’ we again have $(E_y)_{\text{eff}} \sim 0$ with the magnetizations orthogonal to each other as in ‘‘B.’’ The abrupt switching of the magnetization of each layer in the trilayer system results in a characteristic change of R_{xy} that allows us to track the relative configuration of magnetization

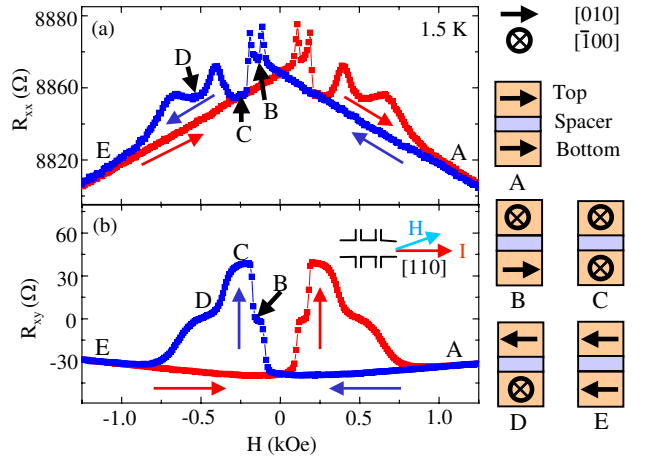


FIG. 3: Magnetic field dependence of (a) R_{xx} and (b) R_{xy} at $T = 1.5\text{ K}$ in device B4. The data are taken in the CIP geometry with $\vec{j} \parallel [110]$ and \vec{H} aligned 15° off [110]. Arrows in (b) represent relative magnetizations of the top and bottom $\text{Ga}_{1-x}\text{Mn}_x\text{As}$ layers. Panels (c) and (d) depict the configurations of magnetization and magnetic field when $\varphi = 45^\circ$ and $\varphi = 135^\circ$, respectively.

orientations. As shown in Fig. 3, the distinctive features in $R_{xx}(H)$ are then directly correlated with the magnetization configuration of the $\text{Ga}_{1-x}\text{Mn}_x\text{As}$ layers, with a minimum R_{xx} when the magnetizations are aligned parallel, and an enhanced R_{xx} for non-collinear configurations.^{15,16}

However, Fig. 3 also shows that the detailed shape of the MR in these FMS spin valves is more complex than that found in most metallic spin valves, showing a double peak structure. This feature arises from an interesting interplay between the spin valve effect and the intrinsic AMR of an individual $\text{Ga}_{1-x}\text{Mn}_x\text{As}$ layer, leading to a MR *valley* exactly where a pure spin valve effect would lead to a MR peak. This behavior may be qualitatively explained using the magnetoimpurity scattering model^{9,17} which shows that $R_{xx}(H)$ for a single $\text{Ga}_{1-x}\text{Mn}_x\text{As}$ layer decreases abruptly when the magnetization first switches upon field reversal (as in Fig. 1(c)). This occurs because of a discontinuous change in $\rho_\perp = a - b|\vec{B}| = a - b|\vec{H} + \vec{M}|$, where both a and b are positive parameters. Hence, when the magnetization of the top $\text{Ga}_{1-x}\text{Mn}_x\text{As}$ layer in a spin valve device switches, $|\vec{B}| = |\vec{H} + \vec{M}|$ increases, ρ_\perp decreases and R_{xx} decreases (Eq. 1). As a consequence, the enhanced MR due to the spin valve effect is opposed by the intrinsic single layer AMR precisely when the layers switch from parallel to orthogonal configurations, resulting in a MR valley. The spin valve effect in these semiconductor-based trilayers has two possible microscopic origins: SDS occurring at

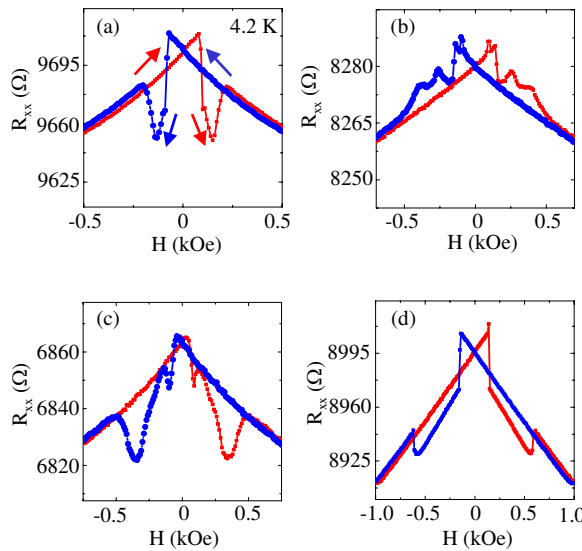


FIG. 4: Magnetic field dependence of R_{xx} and R_{xy} at $T = 4.2\text{ K}$ in trilayer devices with (a) 2 nm spacer (device A), (b) 5 nm spacer (device B3) and (c) 10 nm spacer (device C). All three trilayers are subject to 60 minute annealing at 190°C . Panel (d) shows data for the as-grown epilayer (device D). The data are all taken in the CIP geometry with $\vec{j} \parallel [110]$ and \vec{H} aligned 20° off [110].

the interfaces between layers and SDS due to impurities present in the bulk of the layers. Since the diffusion length of holes in $\text{Ga}_{1-x}\text{Mn}_x\text{As}$ is expected to be only a few nm and the spacer layer thickness is 5 nm, contributions from SDS in the bulk should make a very small contribution to the MR. Instead, we expect that SDS at the interfaces should be the dominant mechanism for the spin valve effect. This interpretation is supported by the observed enhancement of the spin valve effect by annealing: we speculate that the annealing leads to compositional disorder at the interfaces (possibly due to migration of both Mn and Be atoms), resulting in an increase of SDS at the interfaces. Such a mechanism has been suggested as an explanation for annealing-enhanced GMR in metallic multilayers.¹⁸ Within such a picture, the spin

valve effect should show a non-monotonic dependence on annealing time due to the trade-off between the enhancement of SDS due to Mn diffusion into the spacer layer and reduction of spin scattering due to Be migration in to the $\text{Ga}_{1-x}\text{Mn}_x\text{As}$ layers. This is supported by our data, showing that 90-minute annealing has a bigger spin valve effect than shorter and longer annealing times.

The role of SDS at interfaces is also consistent with the dependence of the observed spin valve effect on the thickness of the spacer layer. This is shown in Figs. 4 (a) - (d) where we compare the field dependence of R_{xx} for devices A, B3, C (all annealed for 60 minutes at 190°C) and the (as-grown) control sample D. The data show that the spin valve effect is absent in devices with the thinnest (2 nm) spacer layer (Fig. 4(a)), where the behavior is similar to that of the control epilayer (Fig. 4(d)). We attribute this to a coupling between the $\text{Ga}_{1-x}\text{Mn}_x\text{As}$ layers which makes the trilayer act like a single layer. The spin valve effect is strongest in devices with the 5 nm spacer (Fig. 4(b)) and absent in devices with the thickest (10 nm) spacer (Fig. 4(c)). The latter is consistent with an anticipated hole spin diffusion length of several nm. We note that qualitative features of this spacer thickness dependence has been reproduced in devices fabricated from different wafer runs of nominally identical samples.

In conclusion, we have observed the spin valve effect in all-semiconductor $\text{Ga}_{1-x}\text{Mn}_x\text{As}/\text{Be}:\text{GaAs}/\text{Ga}_{1-x}\text{Mn}_x\text{As}$ trilayer devices and found that annealing is critical to its observation. The dependence of the spin valve effect on annealing time and spacer thickness suggests that the spin valve effect principally arises from the spin-dependent scattering at interfaces. This first demonstration of the spin valve effect in (Ga,Mn)As based trilayers provides an alternative route towards current-driven spin torque in ferromagnetic semiconductor devices, instead of using tunneling structures.⁶ Further, these all-semiconductor spin valves give access to a very different regime of parameter space for studying spin valve behavior compared to metallic systems and may provide fundamental new insights into the underlying physics.

This research has been supported by grant numbers ONR N0014-05-1-0107, University of California-Santa Barbara subcontract KK4131, and NSF DMR-0305238 and -0401486.

* Electronic address: nsamarth@psu.edu

¹ S. A. Wolf, D. D. Awschalom, R. A. Buhrman, J. M. Daughton, S. von Molnar, M. L. Roukes, A. Y. Chtchelkina, and D. M. Treger, *Science* **294**, 1488 (2001).

² A. H. Macdonald, P. Schiffer, and N. Samarth, *Nature (Materials)* **4**, 195 (2005).

³ M. Tanaka and Y. Higo, *Phys. Rev. Lett.* **87**, 026602 (2001).

⁴ S. H. Chun, S. J. Potashnik, K. C. Ku, P. Schiffer, and

N. Samarth, *Phys. Rev. B* **66**, 100408(R) (2002).

⁵ K. F. Eid, M. B. Stone, K. C. Ku, O. Maksimov, P. Schiffer, N. Samarth, T. C. Shih, and C. J. Palmstrom, *Appl. Phys. Lett.* **85**, 1556 (2004).

⁶ D. Chiba, Y. Sato, T. Kita, F. Matsukura, and H. Ohno, *Phys. Rev. Lett.* **93**, 216602 (2004).

⁷ M. N. Baibich, J. M. Broto, A. Fert, F. N. Vandau, F. Petroff, P. Etienne, G. Creuzet, A. Friederich, and J. Chazelas, *Phys. Rev. Lett.* **61**, 2472 (1988).

⁸ E. Y. Tsymbal and D. G. Pettifor, *Perspectives of giant magnetoresistance* (Academic Press, 2001), vol. 56 of *Solid State Physics*, pp. 113–237.

⁹ S. T. B. Goennenwein, S. Russo, A. F. Morpurgo, T. M. Klapwijk, W. Van Roy, and J. De Boeck, Phys. Rev. B **71**, 193306 (2005).

¹⁰ H. X. Tang, R. K. Kawakami, D. D. Awschalom, and M. L. Roukes, Phys. Rev. Lett. **90**, 107201 (2003).

¹¹ G. Xiang, A. W. Holleitner, B. L. Sheu, F. M. Mendoza, O. Maksimov, M. B. Stone, P. Schiffer, D. D. Awschalom, and N. Samarth, Phys. Rev. B **71**, 241307(R) (2005).

¹² K. W. Edmonds, P. Boguslawski, K. Y. Wang, R. P. Cam- pion, S. N. Novikov, N. R. S. Farley, B. L. Gallagher, C. T. Foxon, M. Sawicki, T. Dietl, et al., Phys. Rev. Lett. **92**, 037201 (2004).

¹³ D. Chiba, K. Takamura, F. Matsukura, and H. Ohno, Appl. Phys. Lett. **82**, 3020 (2003).

¹⁴ M. B. Stone, K. C. Ku, S. J. Potashnik, B. L. Sheu, N. Samarth, and P. Schiffer, Appl. Phys. Lett. **83**, 4568 (2003).

¹⁵ L. M. Li and F. C. Pu, Phys. Rev. B **51**, 3640 (1995).

¹⁶ J. C. Slonczewski, Phys. Rev. Lett. **67**, 3172 (1991).

¹⁷ E. L. Nagaev, Physics Reports **346**, 388 (2001).

¹⁸ P. A. E. Jonkers, Phys. Rev. B **64**, 134427 (2001).